Optimization of an indirect heating process forfood fluids through the combined use of CFD andResponse Surface Methodology

Proof Central

Please use this PDF proof to check the layout of your article. If you would like any changes to be made to the layout, you can leave instructions in the online proofing interface. First, return to the online proofing interface by clicking "Edit" at the top page, then insert a Comment in the relevant location. Making your changes directly in the online proofing interface is the quickest, easiest way to correct and submit your proof.

Please note that changes made to the article in the online proofing interface will be added to the article before publication, but are not reflected in this PDF proof.

Food and Bioproducts Processing xxx (2021) xxx–xxx

Contents lists available at ScienceDirect

Food and Bioproducts Processing

journal homepage: www.elsevier.com/locate/fbp

Optimization of an indirect heating process for food fluids through the combined use of CFD and Response Surface Methodology

Natalya Lysova, Federico Solari, Giuseppe Vignali*

Department of Engineering and Architecture, University of Parma, viale delle Scienze 181/A, Campus Universitario, 43124 Parma, Italy

ARTICLE INFO

Article history:
Received 17 August 2021
Received in revised form 22 October 2021
Accepted 26 October 2021
Available online xxx

Keywords:
Computational Fluid Dynamics
Heat exchanger
Non Newtonian fluids
Reduced order modeling
Digital Twin

ABSTRACT

The behavior of a counter-current tube-in-tube heat exchanger for fluid foods, was simulated under different operating conditions with a Computational Fluid Dynamics (CFD) parametric study. Three input parameters (product velocity $v_{p,in}$, inlet product temperature $T_{p,in}$ and inlet water temperature $T_{w,in}$) and two output parameters (outlet product temperature $T_{p,out}$ and pressure drop across the heat exchanger Δp) were chosen. The results highlighted that the relative impact of $v_{p,in}$ on Δp was positive (93%), while higher $T_{p,in}$ and $T_{w,in}$ yielded lower pressure drop values (−3% and −4%, respectively). $T_{p,out}$ was influenced positively by inlet product (62%) and water (22%) temperatures, and negatively by $v_{p,in}$ (−16%).

A Response Surface (RS) was then generated and validated with a suitable experimental campaign. A good agreement was found between the simulated and the experimental results: $T_{p,out}$ and Δp have been calculated with mean errors of 0.85 K and 628 Pa, respectively, thereby confirming the potential value of the RS as a Reduced Order Model, which could be used to develop a Digital Twin of the device. This modelling approach leads to a significant state-of-the-art improvement, allowing m the results of the CFD simulations to be ready-to-use, and granting deeper knowledge and finer control of the system.

1. Introduction

One of the biggest challenges in defining heat treatment for a food product is to guarantee food safety by preserving the organoleptic characteristics of the product itself as much as possible. In particular, in thermal treatment of fluid products the geometric features of the heating device and the process parameter settings are crucial to reaching the desired temperatures in the most rapid and uniform way. To achieve this goal, it is essential to have a deep understanding of the rheological behaviour of the product and its dependence on the process parameters, since it can strongly influence the flow patterns, thereby affecting system pressure drop and heat transfer performance (Chhabra and Richardson, 1999). Moreover, most of the fluid foods are non-Newtonian and their viscosity strongly depends not only on the temperature but also on the shear rate. The rheological behaviour of these fluids can be described through mathematical models, such as Power Law, Bingham, Herschel–Bulkley, Cross and Carreu models (Steffe, 1996).

In industrial applications, the desired pasteurization or sterilization temperature of the fluid food can be reached using a heating medium or electric current. In the former case, the heat transfer can be either direct, with the water vapour being directly injected or infused into the product, or indirect, where the product does not come into contact with the heating medium, since they are separated by a metallic wall (Singh and Heldman, 2014). In the case of electric ohmic heating, heat is internally generated within the material being processed due to its natural electrical resistance, thanks to an electric current passing through it (Maloney and Harrison, 2016).

In the case of viscous food products, the flow regime inside conventional heat transfer devices is usually laminar, lead-

* Corresponding author.
E-mail address: federico.solari@unipr.it (F. Solari).

https://doi.org/10.1016/j.fbp.2021.10.010
0960-3085/© 2021 Published by Elsevier B.V. on behalf of Institution of Chemical Engineers.

Please cite this article in press as: Lysova, N., et al., Optimization of an indirect heating process for food fluids through the combined use of CFD and Response Surface Methodology. Food Bioprod Process (2021), https://doi.org/10.1016/j.fbp.2021.10.010

ing to a low heat transfer coefficient. In order to achieve a more efficient heat treatment, many enhancement methods have been developed, consisting in various techniques aiming to reduce the thermal resistance by increasing the effective heat transfer surface area or by generating turbulence (Maradiya et al., 2018). However, most passive heat transfer enhancement techniques cannot be applied when the fluid is highly viscous or when it contains large solid pieces, because the inserts would damage the particles and the corrugation would make the heat exchanger surface difficult to clean. To avoid these problems and achieve an efficient thermal treatment, ohmic heating is sometimes preferred for high viscous and heat-sensitive fluids, low flow rates and food containing large particulates. For all other applications the conventional heating with heat exchangers is adopted because of its cost-effectiveness, flexibility, ease of use and management.

Many studies on heat exchangers based on Computational Fluid Dynamics (CFD) can be found in the literature. The numerical simulations allow detailed insight into the flow patterns and distributions of the physical properties in every point of the simulated domain. Moreover, this approach allows the assessment of what-if scenarios by changing both geometric and operating parameters in order to optimize the overall performance of the process and reduce waste and costs, without the need for an expensive and time-consuming experimental campaign. CFD applications in the sector of food thermal treatment include studies on pasteurization of fruit puree containing pieces (D'Addio et al., 2014), thermal treatment of a commercial juice inside a tube with a curved elbow (Córcoles et al., 2020), sterilization process, and subsequent nutrient degradation, of blackberry juice (Dantas and Gut, 2018), and enhancement of the olive oil extraction process by thermal conditioning of olive paste (Perone et al., 2021).

Although the CFD is widely used, it appears to be extremely time-consuming and requires an intensive computational resource; for this reason, there have been few applications of CFD for real-time control of industrial processes to date. Nowadays, however, increasing attention is being paid to the design of Digital Twins of food processes, which allow monitoring and controlling the production systems (Tagliavini et al., 2019; Verboven et al., 2020). Response Surface Methodology (RSM) could be effectively adopted for the results of CFD simulations to be ready to use within an industrial control process (Mishra and Ein-Mozaffari, 2021). Response surfaces can also be used to optimize the performances of devices and processes by modifying the values of input parameters of the CFD simulations and evaluating their effects on the output responses of interest.

Applications of RSM in food industry include formulation procedures, drying and blanching processes, and production of microbial enzymes and other metabolites (Yolmeh and Jafari, 2017). Khodashenas and Jouki (2020) used RSM to perform an evaluation of the effects of different gums (Gellan, Xanthan and Quince seed gums) on the stability, probiotic viability and qualitative properties of a drinkable dairy product. Jouki et al. (2014) applied RS methods to investigate the effects of the extraction conditions on the antioxidant activity and the functional properties of quince seed mucilage. Jha and Prasad (1996) used RSM to determine the combination of conditions and operations that allowed optimization of Gorgon nut processing. Dantas and Gut (2018) generated a Response Surface starting from a mathematical model of a double pipe heat exchanger in order to illustrate the dependence of microbiological and nutritional quality on product flow rate and heating medium temperature.

Fig. 1 – Pilot plant set-up.

In the case of heat exchangers, RSM has been used to optimize heat transfer coefficients and friction factors by modifying the geometric features of pipes and inserts and the operating parameters. Some authors (Han et al., 2015) modelled different pipe corrugation geometries, while others simulated twisted tape inserts by varying the features of sinusoidal tape (Yu et al., 2019), modifying cut geometries (Kola et al., 2021) or modelling new configurations of combined vortex generators (Arjmandi et al., 2020). Finally, Liu et al. (2021) evaluated the performance of a coiled tube-in-tube heat exchanger with different coil configurations.

In this study the thermal treatment of a non-Newtonian product flowing through a counter-current tube-in-tube heat exchanger (Bottani et al., 2020) has been evaluated using a CFD simulation. The product tested was a mixture of 0.1 wt% Gellan gum powder (Fialho et al., 2008) and water, whose rheological behavior was assessed at different temperatures and resulted to be pseudo-plastic. A parametric study was defined to characterize the device under different operating conditions. Product flow rate and inlet temperature, along with inlet water temperature, were defined as input parameters, while outlet product temperature and pressure drop across the heat exchanger were defined as output parameters. The simulation results were finally validated with a suitable experimental campaign on the pilot plant. The Response Surface obtained from the parametric study aims to be used to develop a Digital Twin of the system, and to rapidly predict the behavior of the device as a function of the input operating conditions. This approach could improve the current state-of-the-art, since it would allow using the results of CFD simulations for advanced control of industrial plants.

2. Materials and methods

2.1. Equipment

The pilot plant consists in a tubular heat exchanger for preheating of fluid foods that can process up to 2500 l/h of viscous products containing particles with a size up to 10 mm. The plant is equipped with auxiliary systems that supply steam, electricity, water and compressed air to each machine. The system is controlled by a Programmable Logic Controller (PLC) and the process settings can be adjusted from the control panel by means of a Human-Machine Interface (Fig. 1). Q5

As stated before, this study focuses on modeling the heating of a fluid food achieved through a tube-in-tube heat exchanger where the product flows through the inner tube,

Please cite this article in press as: Lysova, N., et al., Optimization of an indirect heating process for food fluids through the combined use of CFD and Response Surface Methodology. Food Bioprod Process (2021), https://doi.org/10.1016/j.fbp.2021.10.010

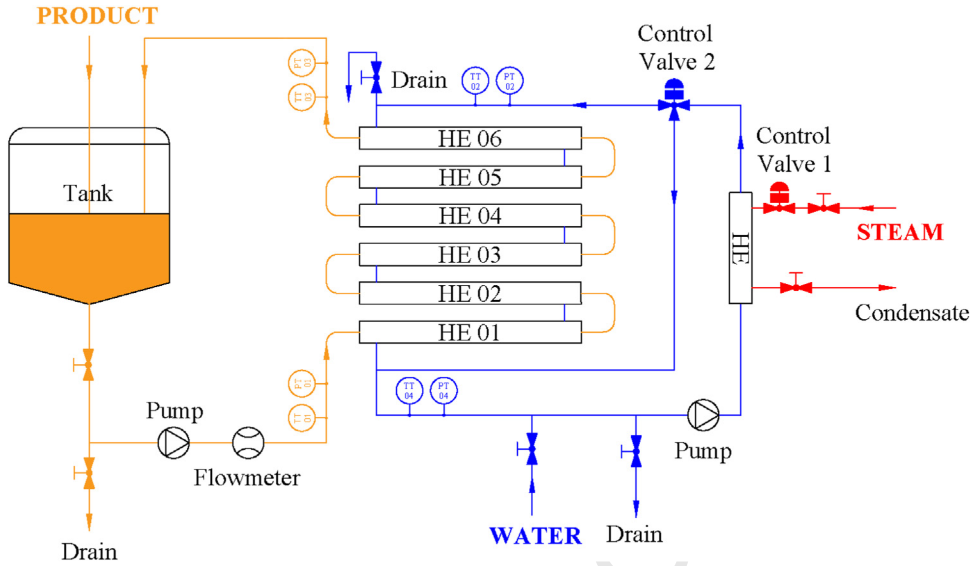

Fig. 2 – Schematic representation of the pilot plant configuration.

while the water flows counter-current in the outer shell tube. The machine consists of six horizontal linear heating modules, each approximately 4 m long, arranged in a vertical configuration. The inner pipes of consecutive modules are connected with 180° bends, while the outer shell pipes are connected with vertical flange connections. Both inner and outer pipes are made of stainless steel.

The product, initially stored in a stainless steel storage tank equipped with a mixer, is moved by means of a twin-screw volumetric pump, whose flow rate is measured through a mass flowmeter and can be adjusted by regulating the frequency of the power supply with an inverter. The product enters the heat exchanger from the lower section, flows through the inner pipe and exits from the upper section, before being finally recirculated to the storage tank.

The water is moved by means of a centrifugal pump: it enters the tubular heat exchanger from the upper section and flows in the opposite direction to the product. The temperature of the water is raised by indirect contact with steam inside a dedicated heat exchanger.

Both steam and water flow rates can be regulated by means of two control valves (respectively Control Valve 1 and Control Valve 2 in Fig. 2). Valve positions can either be adjusted automatically, by using a Proportional-Integral (PI) controller, so that product and water temperatures remain close to user-defined set-point values, or manually defined by setting a fixed opening percentage. Pressure and temperature of both product and water are evaluated through dedicated sensors at the inlet and outlet sections of the heat exchanger: temperatures are measured with resistance temperature detectors, while pressures are measured using pressure transmitters with flush diaphragm.

The main data of the heat exchanger geometry are reported in Table 1.

The main processing parameters of the pilot plant are summarized in Table 2.

2.2. *Materials*

The product used in this study is a mixture of 0.1 wt % Gellan gum powder and water. Gellan gum is a high molecular weight exopolysaccharide produced via aerobic fermentation by *Sphingomonas elodea*, commonly used as a thickening, stabilizing and emulsifying agent in food industry with European food additive E-number E418. To prepare the mixture, 200 g of biopolymer were added to 200 l of water contained in the storage tank. The content of the tank was continuously agitated by means of a mixer and the product pump was running to incorporate the powder gradually and homogeneously.

Table 1 – Geometrical data of the heat exchanger.

Description	Value	Unit
Number of heating modules	6	–
Total linear section length	3950	mm
Heating section length	3770	mm
Distance between water inlet and outlet axes	3600	mm
Inner pipe diameter	39.8	mm
Inner pipe bends r/D	1.5	–
Outer pipe diameter	73.2	mm
Inner and outer pipe thickness	1.5	mm
Water pipe diameter	57.1	mm

Density, thermal conductivity and specific heat were assumed to be similar to those of water, while viscosity was determined thanks to experimental measurements. In food processing applications involving pipe flow, shear rate values generally range from 10° to $10^3\ s^{-1}$ (Steffe, 1996), with the lowest values at the center of the pipe and the maximum values at the walls. In this study the rheological characterization was performed using a concentric cylinder geometry (Couette cell) mounted on an ARES rheometer (Ta Instruments, New Castle, DE, USA). The dimensions of the geometry were 34 mm cup diameter, 32 mm bob diameter, and 33 mm height. Eight ml of the product were transferred to the rheometer cup using a graduate cylinder and a sample was equilibrated for 2 min before being analyzed (Rinaldi et al., 2018). The measurements were conducted under isothermal conditions, evaluating the shear stress at three temperatures (293.15 K, 313.15 K and 333.15 K), with shear rates ranging from 10 to 300 s^{-1}, with 30 points in logarithmic distribution (Fig. 3).

It can be observed that, especially at low temperatures, the fluid had a slightly non-Newtonian, shear thinning behavior, Q6 which can be described by means of a Power-law model:

$$\tau = K\dot{\gamma}^n \qquad (1)$$

Please cite this article in press as: Lysova, N., et al., Optimization of an indirect heating process for food fluids through the combined use of CFD and Response Surface Methodology. Food Bioprod Process (2021), https://doi.org/10.1016/j.fbp.2021.10.010

Table 2 – Main processing parameters of the pilot plant.

		Unit	Value	
			Min	Max
Product pump	Operating pressure	bar	0	5
Twin-screw pump	Flow rate	m^3/h	0	5
	Viscosity	Pa s	0	0.5
	Particle size	mm	0	10
Water pump	Flow rate	m^3/h	0	12
Centrifugal pump	Prevalence	m	25.5	27.5
	Product density	kg/m^3	1000	
	Product viscosity	Pa s	0.001	

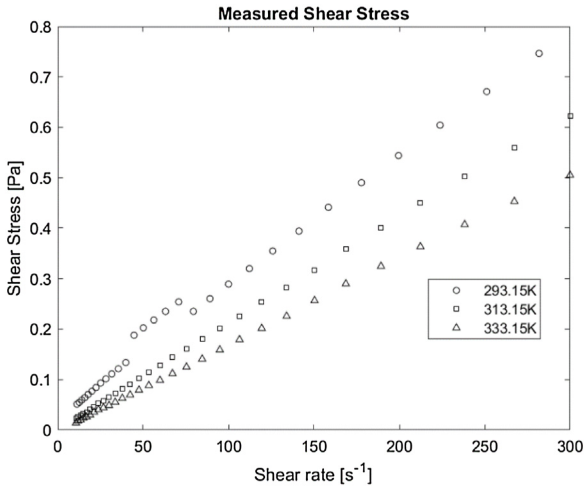

Fig. 3 – Experimentally measured shear stress at three different temperatures.

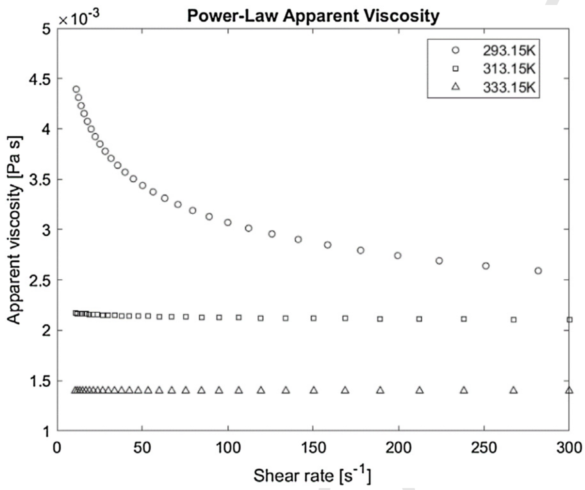

Fig. 4 – Apparent viscosity at the three evaluated temperatures.

where τ is the shear stress, $\dot{\gamma}$ is the shear rate, and K and n are consistency and flow behavior indexes, respectively. Apparent viscosity η of the fluid can be calculated from the shear stress, by means of the following equation (Fig. 4):

$$\eta = \frac{\tau}{\dot{\gamma}} = K\dot{\gamma}^{n-1} \tag{2}$$

A logarithmic transformation of Eq. (1) was performed to evaluate K and n:

$$\ln(\tau) = \ln(K) + n\ln(\dot{\gamma}) \tag{3}$$

Table 3 – Calculated power-law coefficients.

	Unit	293.15K	313.15K	333.15K
K	Pa s^n	0.0065	0.0022	0.0014
n	–	0.84	0.99	1.00

Eq. (3) represents a linear model describing a straight line in the form:

$$y = a + bx \tag{4}$$

where

$$y = \ln(\tau) \tag{5}$$

$$a = \ln(K) \tag{6}$$

$$b = n \tag{7}$$

Parameters a and b are obtained by means of a linear regression aiming to define the least squares regression line by solving the following system of normal equations:

$$\sum_i y_i = aN_m + b\sum_i x_i \tag{8}$$

$$\sum_i x_i y_i = a\sum_i x_i + b\sum_i {x_i}^2 \tag{9}$$

where N_m is the number of experimental measurements, y_i are the natural logarithms of the measured shear stress values, and x_i are log-transformed values of shear rate.

Once the system of equations is solved for a and b, consistency index K can be calculated from Eq. (6), while the flow behavior index n is equal to b.

$$K = \exp(a) \tag{10}$$

The same procedure was used to calculate K and n coefficients at all temperatures considered, and the following values were found (Table 3).

Results show that the product's behavior varies with the temperature: it has a non-Newtonian behavior at low temperatures, while at higher temperatures it behaves like a Newtonian fluid with a viscosity value very close to that of water.

Since the temperature values change significantly within the domain, it is important to consider the temperature dependence of apparent viscosity. The influence of temperature was taken into account using the Arrhenius relationship:

$$\frac{\eta}{\eta_\alpha} = \exp\frac{E_a}{R}\left(\frac{1}{T} - \frac{1}{T_\alpha}\right) \tag{11}$$

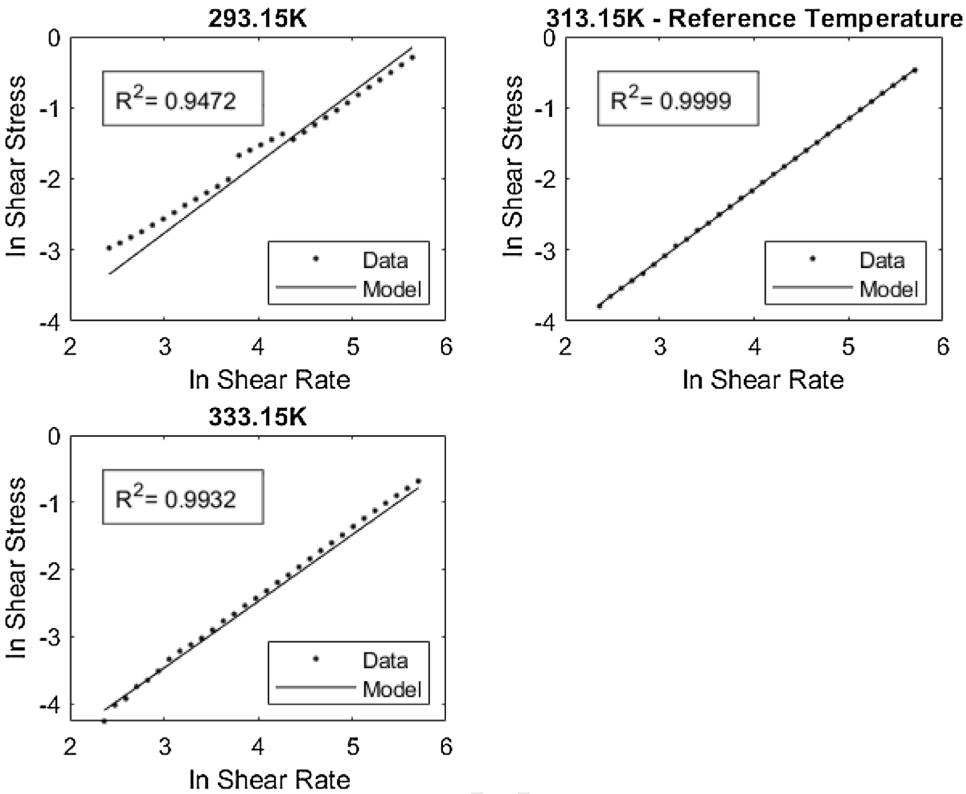

Fig. 5 – Log-transformed data, linear model and calculated coefficients of determination R^2.

where η_α and T_α are reference values, E_a is the energy of activation for viscosity, and R is the universal gas constant. The magnitude of E_a/R was evaluated considering apparent viscosity values at a shear rate of 100 s^{-1}:

$$\frac{E_a}{R} = \frac{\ln\frac{\eta}{\eta_\alpha}}{\frac{1}{T} - \frac{1}{T_\alpha}} \quad (12)$$

The accuracy of the model was assessed by means of the coefficient of determination R^2, calculated with the following equation:

$$R^2 = 1 - \frac{\sum_i (y_i - \hat{y}_i)^2}{\sum_i (y_i - \bar{y})^2} \quad (13)$$

where y_i are the log-transformed values of shear stress, $\bar{y}$ is the mean of y_i values, and $\hat{y}_i$ are the predicted values, calculated as follows:

$$\hat{y}_i = \ln K + n \ln \dot{\gamma} + \frac{E_a}{R}\left(\frac{1}{T} - \frac{1}{T_\alpha}\right) \quad (14)$$

R^2 coefficients were calculated by considering different reference temperatures (Table 4), to determine the combination of temperature values that would grant the best overall model accuracy. The reference temperature chosen in this study was 313.15 K, while the temperature of 293.15 K is used to calculate the value of E_a/R. The calculated model fits the experimental data well, as shown in the following plots (Fig. 5).

The temperature-dependent shear stress, calculated on the basis of K and n coefficients, fits the measured data as illustrated in Fig. 6. The model appears to be more accurate at higher temperatures ($T \geq 313.15$ K).

For the CFD simulations, water and steel too were characterized from a thermodynamic point of view. Materials properties are summarized in Table 5.

2.3. *Flow patterns*

The flow regimes of the two fluids can be estimated by using the Reynolds number value. In the case of water, which is a Newtonian fluid, Reynolds number is calculated as follows:

$$Re = \frac{\rho u D}{\mu} \quad (15)$$

where ρ is the fluid density, u is the velocity, D is the hydraulic diameter of the pipe, and μ is the dynamic viscosity of the fluid.

The flow pattern of the shear-thinning product can be evaluated by means of the generalized Reynolds number equation, proposed by Metzner and Reed (1955):

$$Re_{MR} = \frac{8\rho}{K} w^{2-n} \left(\frac{n}{3n+1}\right)^n R^n \quad (16)$$

where w is the mean velocity of the viscous product and R is the pipe radius.

For practical purposes, the flow pattern inside a pipe can be estimated on the basis of three ranges of Reynolds number: at $Re < 2000$ the flow is laminar and has a parabolic profile; when Re ranges between 2000 and 4000 the flow is in an unstable transition region and can be either laminar or turbulent, with the critical Re_{CR} at which the transition begins to be influenced by fluid properties and geometric features of the pipe; at $Re > 4000$ turbulent flow is dominant and the flow profile becomes fairly flat (LaNasa and Upp, 2014).

As for the processing parameters of the pilot plant, the Reynolds numbers calculated for the two fluids at different

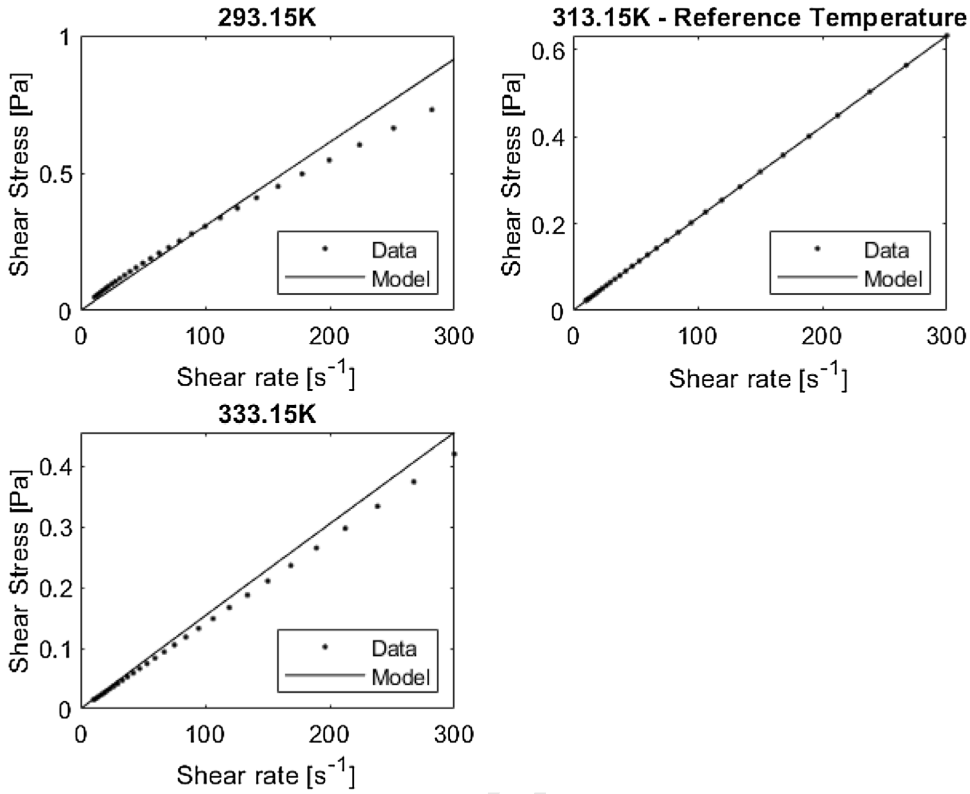

Fig. 6 – Experimental data and power-law temperature-dependent model.

Table 4 – Accuracy of the temperature-dependent viscosity model using different values of reference temperature (T_a) and different temperatures (T) for the evaluation of E_a/R.

T_α [K]	313.15	313.15	293.15	293.15	333.15	333.15
T [K]	293.15	333.15	313.15	333.15	293.15	313.15
E_a/R [K]	1703	1197	1703	1466	1466	1197
R^2 at 293.15K	0.9472	0.8999	0.9924	0.9924	0.9113	0.8518
R^2 at 313.15K	0.9999	0.9999	0.9682	0.9565	0.9973	0.9962
R^2 at 333.15K	0.9932	0.9955	0.9602	0.9472	0.9988	0.9988
Mean R^2	0.9801	0.9651	0.9736	0.9654	0.9691	0.9489

Table 5 – Properties of water, stainless steel and product.

	Viscous product	Water	Stainless steel
Thermodynamic state	Fluid	Fluid	Solid
Density	998.2 kg/m^3	998.2 kg/m^3	8030 kg/m^3
Specific heat	4182 J/kg K	4182 J/kg K	502 J/kg K
Thermal conductivity	0.6 W/m K	0.6 W/m K	16.3 W/m K
Dynamic viscosity	–	0.001 Pa s	–
Consistency index (K)	0.0022 Pa s^n	–	–
Flow behavior index (n)	0.99	–	–
Energy of activation	14.2 kJ/mol	–	–
Reference temperature	313.15 K	–	–

Table 6 – Fluid velocities and calculated Reynolds numbers.

	Pump flow rate [m^3/h]	Uniform velocity on the section [m/s]	Reynolds number Re	Generalized Reynolds number Re_{RM}
Water	12	1.16[a]	18,519	–
Product	1	0.22	–	4164
	2	0.44	–	8386
	3	0.66	–	12,630
	4	0.88	–	16,888
	5	1.11	–	21,157

[a] Mean water velocity on the annular area of the outer pipe.

Please cite this article in press as: Lysova, N., et al., Optimization of an indirect heating process for food fluids through the combined use of CFD and Response Surface Methodology. Food Bioprod Process (2021), https://doi.org/10.1016/j.fbp.2021.10.010

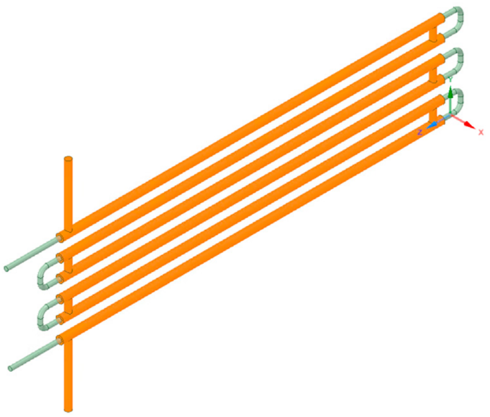

Fig. 7 – Geometry of the heat exchanger, with two separate bodies for the inner and outer pipes.

flow rates are reported in Table 6. It appears that the flow is turbulent for both product and water.

2.4. *Numerical simulation*

Methods for solving heat transfer problems for non-Newtonian fluids in turbulent conditions can be found in the literature (Shenoy, 2018). However, these methods are effectively applicable only if the boundary conditions and the rheological characteristics of the fluid are constant in space and time.

In our case, the rheological characteristics of the product resulted to be extremely sensitive to temperature, which, for both fluids considered, changes from point to point across the heat exchanger. In this case, therefore, a numerical simulation can better reproduce the real situation.

2.4.1. *Geometry and mesh*

In order to perform the numerical simulation of the thermal treatment, a 3D model of the heat exchanger was generated with ANSYS SpaceClaim. The model reproduced the entire machine's geometry and consisted of two distinct bodies: one for the inner fluid domain (product) and one for the outer fluid domain (water). The contribution of the solid domain (stainless steel pipe) was considered as the conductive resistance of a thin stainless steel wall at the interface between the two fluid domains.

The following assumptions were made:

- In order to have fully developed flow profiles at the inlet areas of the heat exchanger, additional linear sections were modelled for inner pipes;
- The inner fluid domain (product) was split into several sections in order to set different boundary conditions for the heating zones and the bends;
- The outer fluid domain (water) was divided into linear sections and T-junction sections in order to facilitate the generation of the computational grid;
- A shared topology option was set for both inner and outer fluid domains in order to obtain matching grids on consecutive sections of the bodies (Fig. 7).

To reduce the computational cost of the simulation, the thermal treatment inside the heat exchanger was considered to be overall symmetrical, thereby allowing modelling only half of the device geometry (Fig. 8).

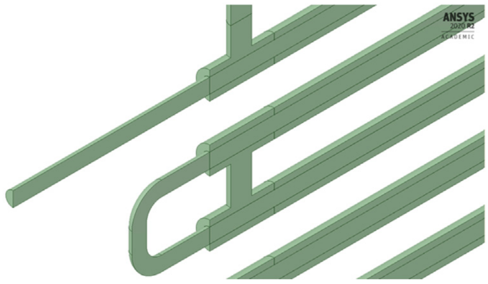

Fig. 8 – Heat exchanger geometry cut in half to reduce the computational cost of the simulations.

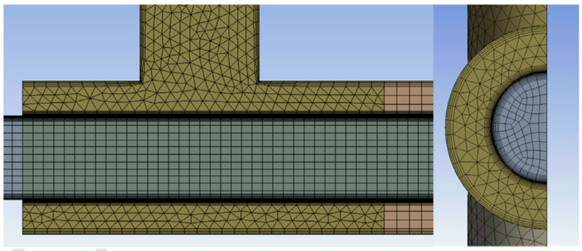

Fig. 9 – Details of the selected mesh.

The grid generation for the two fluid domains was performed with ANSYS Meshing in order to define a finite number of control volumes. A structured hexahedral mesh was created for the fluid product domain, while in the water domain a structured mesh was created in the linear sections, and an unstructured mesh was used within the T-junctions.

Special attention was paid to the near-wall regions in order to obtain accurate information about the heat transfer process. Ten inflation layers, with a first layer thickness of 10^{-4} m and 1.2 growth rate, were generated at each side of the interface for both product and water domains.

A grid sensitivity analysis was carried out to examine the influence of the mesh size on the simulation results. Five different grids with an increasing number of elements was tested, and the outlet product temperature and pressure drop values calculated were then compared. The differences in the results obtained, especially the outlet temperatures, were very small, so the grid for the study was determined on the basis of the pressure drop values and the computation time (Table 7).

Mesh 3 resulted to be the best choice since a higher number of elements provided no significant improvement in the results, while strongly increasing computation time (Fig. 9).

2.4.2. *Governing equations*

In order to model the thermal treatment inside the heat exchanger, ANSYS Fluent 2020 R2 was used to solve the governing equations for the defined fluid domains. According to ANSYS Fluent Theory Guide, the numerically solved Navier–Stokes equations are defined as follows.

The continuity equation for o mass conservation is:

$$\frac{\partial \rho}{\partial t} + \nabla (\rho \vec{v}) = 0 \tag{17}$$

where t is time, ρ is the density of the fluid, and $\vec{v}$ is the overall velocity vector.

Conservation of momentum is described by:

$$\frac{\partial}{\partial t} (\rho \vec{v}) + \nabla (\rho \vec{v} \vec{v}) = -\nabla p + \nabla (\tau) + \rho \vec{g} + \vec{F} \tag{18}$$

Please cite this article in press as: Lysova, N., et al., Optimization of an indirect heating process for food fluids through the combined use of CFD and Response Surface Methodology. Food Bioprod Process (2021), https://doi.org/10.1016/j.fbp.2021.10.010

Table 7 – Comparison of simulation results using different grids.

Grid	Element size [mm]	Number of elements [mil]	Computation time [h]	Pressure drop [mbar]
1	7	1.5	3	150.02
2	6	2.2	5.5	149.84
3	5	3.5	7	149.71
4	4	4.6	10	149.70
5	3	7.8	17	149.69

Table 8 – Input and output parameters of the parametric study.

Parameter	Name	Variable	Description	Unit
Input	P1	x_1	Inlet product temperature	K
Input	P2	x_2	Product velocity on the inlet area	m/s
Input	P3	x_3	Inlet water temperature	K
Output	P4	y_1	Outlet product temperature	K
Output	P5	y_2	Pressure drop	Pa

where p is the static pressure, $\rho\vec{g}$ is the gravitational body force, and $\vec{F}$ considers external body forces. The stress tensor τ is defined as follows:

$$\tau = \mu\left[\left(\nabla\vec{\upsilon} + \nabla\vec{\upsilon}^{T}\right) - \frac{2}{3}\nabla(\vec{\upsilon}I)\right] \tag{19}$$

where μ is the molecular viscosity and I is the unit tensor.

Since the problem includes heat transfer, the energy equation is solved and defined as:

$$\frac{\partial}{\partial t}(\rho E) + \nabla\left(\vec{\upsilon}\left(\rho E + p\right)\right) = \nabla\left(k\nabla T\right) - \nabla\left(\tau\vec{\upsilon}\right) \tag{20}$$

where total energy E is defined as:

$$E = h - \frac{p}{\rho} + \frac{\upsilon^2}{2} \tag{21}$$

In the energy equations mentioned above, k is the thermal conductivity of the material and h is the enthalpy.

2.4.3. *Boundary conditions*

The simulated three-dimensional flow was incompressible, so a pressure-based solver was used for the study, and the gravity option enabled.

Uniform axial velocity and temperature values were defined on the inlet areas for both fluid domains. The outlet areas were defined as pressure outlets, with gauge pressure set to zero in order to calculate the pressure drop inside the heat exchanger.

A symmetry boundary condition was applied to all the surfaces lying in the plane of symmetry. A no-slip condition was set at the walls. The interface between the two fluid domains was defined as a coupled two-sided wall made of steel, with wall thickness equal to 2 mm. The walls in contact with the external environment were considered to be adiabatic.

The simulations were carried out in steady-state conditions and the convergence criterion was set at 10^{-6}. A coupled scheme was used for pressure-velocity coupling during the numerical solution of the governing equations. The gradients were computed according to the Least Squares Cell-Based method. PRESTO! scheme was used to interpolate pressure since it is suitable for flows in curved domains. A second-order upwind discretization scheme was used for energy and turbulent flow equations, while a first-order upwind was used for the momentum equation to improve the convergence of the solution.

In addition, Shear-Stress Transport (SST) k-ω turbulence model was used to solve the turbulent flow numerically. SST k-ω model is a linear combination of k-ε and k-ω models activated for the free stream regions and near-wall zones, respectively, in order to overcome the limits of both models (Menter, 1994).

2.4.4. *Parametric study*

A parametric study was defined as shown in Table 8 to model the behavior of the heat exchanger under different operating conditions. Product flow rate, and inlet product and water temperatures were selected as input parameters. Outlet product temperature and pressure drop through the heat exchanger were chosen as output parameters. The results of the parametric study, calculated in a finite number of Design Points (DPs), were used to generate a Response Surface to estimate the values of the output variables (responses) in all the points of the simulated domain.

2.5. *Response surface generation*

Response Surface Methodology (RSM) is a collection of mathematical and statistical techniques used to model and analyze problems in which a dependent response of interest (y_k) is a function of a set of independent explanatory factors (x_i) (Montgomery, 2001). In this study there are three independent factors (x_1, x_2, x_3), so a generic estimated response could be expressed as

$$y_k = f\left(x_1, x_2, x_3\right) + \varepsilon \tag{22}$$

where ε is the error observed in the response y_k. The graphical three-dimensional representation of the response, plotted against two independent factors of choice, is called “Response Surface”.

The simulated DPs where the responses should be numerically evaluated were defined by means of a proper Design of Experiments (DOE). The first step was the definition of the experimental domain, performed by choosing the range for each input factor as summarized in Table 9. Five levels of coded factors cf were defined in a dimensionless range from $-\alpha$ to α, and the actual values of the input parameters were then calculated using Eq. (23). Coded and actual input factor values are reported in Table 10.

$$x_i = \frac{cf\left(x_{i,1} - x_{i,-1}\right)}{2} + \bar{x}_i \tag{23}$$

Table 9 – Ranges of the three input factors that define the experimental domain.

Factors		Natural variables	
Name	Unit	Min	Max
x_1	K	293.15	333.15
x_2	m/s	0.221	1.105
x_3	K	323.15	373.15

Table 10 – Five-level coded input variables.

Factors	Coded factors				
Name	$-\alpha$	−1	0	1	α
x_1	293.15	296.90	313.15	329.41	333.15
x_2	0.22	0.30	0.66	1.02	1.11
x_3	323.15	327.82	348.15	368.48	373.15

Table 11 – Design points of the parametric study based on face-centered CCD model.

	Input factors			
Design point	x_1	x_2	x_3	Point type
1	0	0	0	Central point
2	-α	0	0	Axial points
3	α	0	0	
4	0	-α	0	
5	0	α	0	
6	0	0	-α	
7	0	0	α	
8	−1	−1	−1	Factorial points
9	1	−1	−1	
10	−1	1	−1	
11	1	1	−1	
12	−1	−1	1	
13	1	−1	1	
14	−1	1	1	
15	1	1	1	

α value is equal to 1.23 and was calculated by minimizing a measure of non-orthogonality, known as the Variance Inflation Factor (VIF) (Ansys Inc., 2017a,b).

The Central Composite Design model (CCD) was selected to define the experimental design for this study since it required fewer simulation runs compared to the Full Factorial Design (FFD) and provided higher accuracy at the extremes of the experimental domain compared to the Box–Behnken Design (BBD). CCD is a second-order polynomial model developed by Box and Wilson (1951) consisting in three-point types: a centre point, two-level factorial points, and axial points at a distance α from the central point. Factorial points estimate linear effects and two-factor interactions, while axial and central points evaluate quadratic effects.

The number of experimental runs N_r can be estimated by (24):

$$N_r = 2^f + 2f + C_p \quad (24)$$

where f is the number of factors and C_p is the central point. The experimental matrix, with the definition of the simulated design points in terms of coded factors, is reported in Table 11.

The experimental 3D domain, defined by the evaluated design points, is shown in Fig. 10.

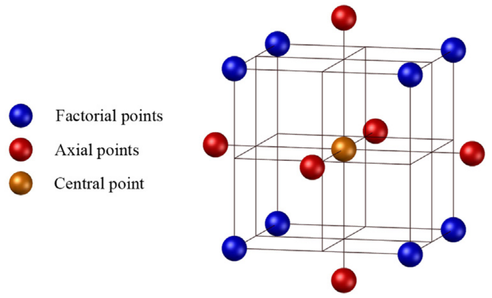

Fig. 10 – Three factor Central Composite Design (CCD) model with five-level variables.

2.6. *Experimental method*

An experimental campaign was conducted on the pilot plant to validate the simulated results. A set-point value for water temperature was defined in the dedicated control panel section after the product was prepared. Automatic regulation of the opening percentage of Control Valve 1 was enabled to raise water temperature to the set-point value and then maintain it stable at that level during the treatment. The opening percentage of Control Valve 2 was set manually at 100% to allow the whole volume of water to flow in the outer pipes of the heat exchanger.

Since the product was continuously recirculated, its temperature at the inlet section of the heat exchanger changed constantly under the influence of the water temperature (see Fig. 2). Therefore, during the experimental validation, the only manually-set parameter was product flow rate, which was changed by adjusting the frequency of the power supply of the pump with an inverter. Different values were tested to verify the reliability of the model under different operating conditions. Phases with constant flow rate, and with sudden and significant changes in flow rate were tested to verify whether the model's responses followed those of the real system, and to assess the extent of any deviations and delays.

3. Results and discussion

3.1. *Simulation results*

The simulation results for the outputs of interest, evaluated at operating conditions defined by the DPs examined, are summarized in Table 12.

Contours of temperature, pressure, shear rate and viscosity, with input parameter values corresponding to the central point of the experimental domain (DP1) are presented in the following figures (Figs. 11–14).

3.2. *Response surface*

A Response Surface was generated starting from the results of the CFD simulations reported in Table 12. RS generation, with relative Analysis of Variance (ANOVA), was carried out in the statistical analysis software Design Expert v.13.

A quadratic model was used to fit the CFD data. The equation for a generic response can be expressed as:

$$\begin{aligned} y_k = {} & \beta_0 + \beta_1{}^{*}v_{p,in} + \beta_2{}^{*}T_{p,in} + \beta_3{}^{*}T_{w,in} + \beta_{12}{}^{*}v_{p,in}{}^{*}T_{p,in} \\ & + \beta_{13}{}^{*}v_{p,in}{}^{*}T_{w,in} + \beta_{23}{}^{*}T_{p,in}{}^{*}T_{w,in} + \beta_{11}{}^{*}v_{p,in}{}^{2} \\ & + \beta_{22}{}^{*}T_{p,in}{}^{2} + \beta_{33}{}^{*}T_{w,in}{}^{2} + \varepsilon \end{aligned} \quad (25)$$

Please cite this article in press as: Lysova, N., et al., Optimization of an indirect heating process for food fluids through the combined use of CFD and Response Surface Methodology. Food Bioprod Process (2021), https://doi.org/10.1016/j.fbp.2021.10.010

Table 12 – Simulation results for the output parameters of interest.

	Input parameters			Output parameters	
DP	P1 $v_{p,in}$ [m s^{-1}]	P2 $T_{p,in}$ [K]	P3 $T_{w,in}$ [K]	P4 Δp [Pa]	P5 $T_{p,out}$ [K]
1	0.66	313.15	348.15	13287.52	337.58
2	0.22	313.15	348.15	9272.69	342.91
3	1.11	313.15	348.15	20504.08	333.68
4	0.66	293.15	348.15	13435.42	330.33
5	0.66	333.15	348.15	13160.27	343.89
6	0.66	313.15	323.15	13521.71	319.84
7	0.66	313.15	373.15	13086.98	356.48
8	0.30	296.89	327.82	9881.18	320.72
9	1.02	296.89	327.82	19557.34	314.66
10	0.30	329.41	327.82	9801.65	328.16
11	1.02	329.41	327.82	18943.92	328.45
12	0.30	296.89	368.48	9728.24	356.21
13	1.02	296.89	368.48	18901.04	340.21
14	0.30	329.41	368.48	9679.40	362.53
15	1.02	329.41	368.48	18445.31	353.90

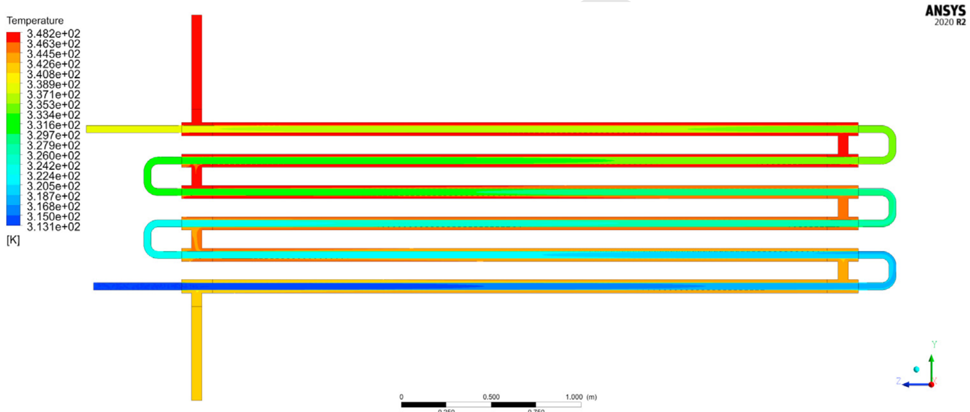

Fig. 11 – Temperature of product and water on the symmetry plane of the heat exchanger.

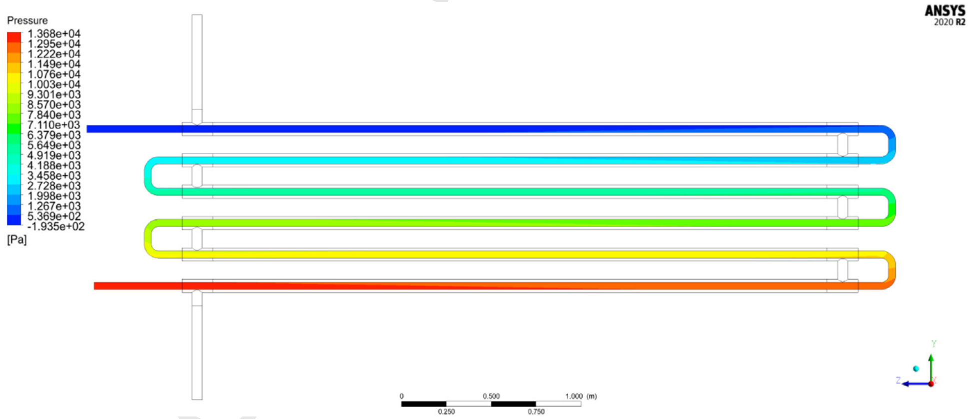

Fig. 12 – Profile of pressure across the heat exchanger.

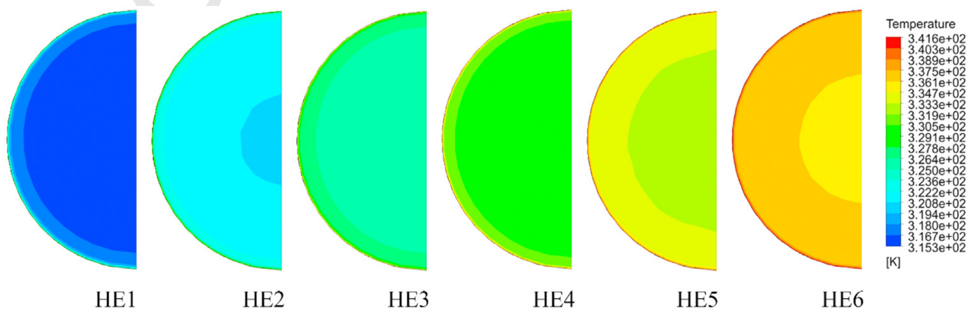

Fig. 13 – Product temperature profiles at the central transversal section of each Heat Exchanger (HE) module.

Please cite this article in press as: Lysova, N., et al., Optimization of an indirect heating process for food fluids through the combined use of CFD and Response Surface Methodology. Food Bioprod Process (2021), https://doi.org/10.1016/j.fbp.2021.10.010

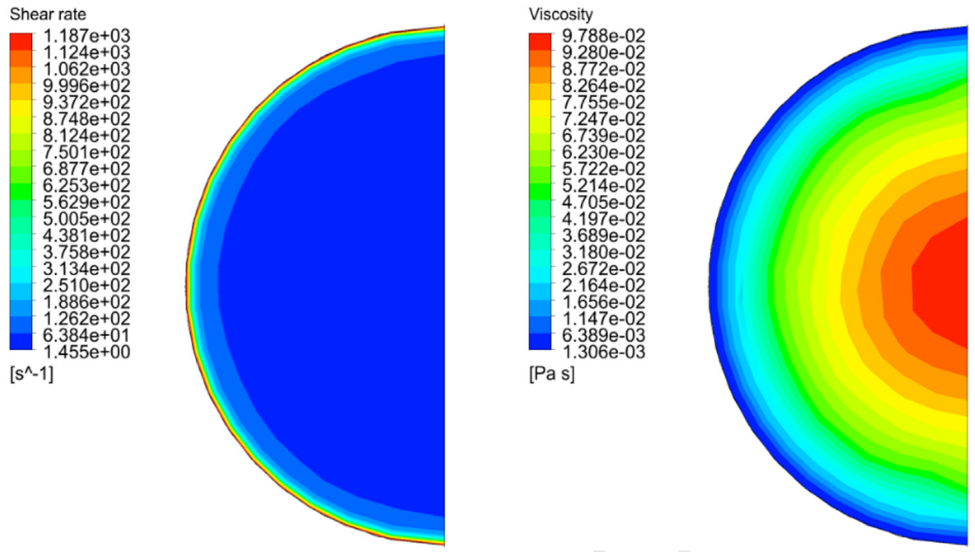

Fig. 14 – Contours of shear rate (left) and shear rate dependent viscosity (right) on a transversal section of the inner pipe.

Table 13 – ANOVA results for the quadratic model –p values calculated for pressure drop and outlet product temperature responses.

	Δp response		$T_{p,out}$ response	
Source	p-Value	Significant	p-Value	Significant
Model	<0.0001	Yes	<0.0001	Yes
$v_{p,in}$	<0.0001	Yes	<0.0001	Yes
$T_{p,in}$	<0.0001	Yes	<0.0001	Yes
$T_{w,in}$	<0.0001	Yes	<0.0001	Yes
$v_{p,in} \times T_{p,in}$	0.0003	Yes	<0.0001	Yes
$v_{p,in} \times T_{w,in}$	0.0004	Yes	<0.0001	Yes
$T_{p,in} \times T_{w,in}$	0.1354	No	0.24	No
$v_{p,in}{}^2$	<0.0001	Yes	0.028	Yes
$T_{p,in}{}^2$	0.6476	No	0.087	No
$T_{w,in}{}^2$	0.499	No	0.057	No

where β_{ij} are the factor coefficients, and ε, as stated before, is the expected error. In the current study the responses of interest were the pressure drop ($y_1 = \Delta p$) and the outlet product temperature ($y_2 = T_{p,out}$). The ANOVA test was conducted to determine whether the model and its terms were significant for the evaluated responses (Table 13).

A term is considered to be significant if its p-value is less than 0.05. For both estimated responses, the generated quadratic model and all of its terms are significant, except for the product of the two inlet temperatures and their square values. The R^2 coefficients of determination values are very close to 1 for both responses ($R^2_{\Delta p} = 0.9999$, $R^2_{Tp,out} = 0.9998$), meaning that the quadratic model predicts the simulated values very well.

The final equations for outlet product temperature and pressure drop can be expressed in terms of actual input parameters in their original units, using Eq. (25) and the calculated quadratic model coefficients summarized in Table 14. These equations can be used to estimate the system responses for given levels of input factors.

A Local Sensitivity (LS) analysis was performed to understand the relative impact that each input factor has on the estimated response. For a single input parameter (x_i), response (R) sensitivity is calculated as:

$$LS(R, x_i) = \frac{\max(R(x_i)) - \min(R(x_i))}{\max(R) - \min(R)} \tag{26}$$

where $\max(R) - \min(R)$ is the maximum response variation and $\max(R(x_i)) - \min(R(x_i))$ is the maximum response variation due to the changing of factor x_i, with the other input parameters being held constant. If the response value rises as the factor value increases, LS is a positive number, otherwise it is negative (Fig. 15).

As shown in Fig. 16, the pressure drop is mostly influenced by product velocity, while product and water temperatures result to have a lower impact. The strongest positive effect on outlet temperature of the product is given by the water temperature, while an increase in product velocity yields a lower product temperature raise, since the residence time of the fluid inside the heat exchanger decreases.

A graphical representation of the estimated responses can be seen in Fig. 17: the pressure drop response is plotted as a function of inlet product temperature and velocity, while the outlet product temperature is represented as a function of the inlet temperatures of water and product.

Contour plots of the estimated response for pressure drop, expressed in Pa, are shown in Fig. 18, for different combinations of $T_{p,in}$ and $v_{p,in}$. The third factor, specifically $T_{w,in}$, is fixed at three values corresponding to $-\alpha$, 0 and α coded levels. The strong dependence of the pressure drop on the product flow rate is once again evident.

Response surfaces for outlet product temperature, expressed in K, are generated as a function of $T_{p,in}$ and $v_{p,in}$, at 3 fixed values of $T_{w,in}$ (Fig. 19). On the right-hand side of the first contour plot the fluid is considered to flow

Table 14 – Calculated quadratic model coefficients for pressure drop and outlet product temperature responses.

Coefficient	Factor	Pressure drop [Pa]	Outlet product temperature [K]
β_0	–	21257.31	−86.24
β_1	$\upsilon_{p,in}$	13422.97	5.26
β_2	$T_{p,in}$	−40.41	1.05
β_3	$T_{w,in}$	−42.84	0.47
β_{12}	$\upsilon_{p,in}{}^{*}\,T_{p,in}$	−20.12	0.29
β_{13}	$\upsilon_{p,in}{}^{*}\,T_{w,in}$	−15.05	−0.32
β_{23}	$T_{p,in}{}^{*}\,T_{w,in}$	0.07	−4.58e-04
β_{11}	$\upsilon_{p,in}{}^2$	8208.07	3.59
β_{22}	$T_{p,in}{}^2$	0.03	−1.22e-03
β_{33}	$T_{w,in}{}^2$	0.03	9.03e-04

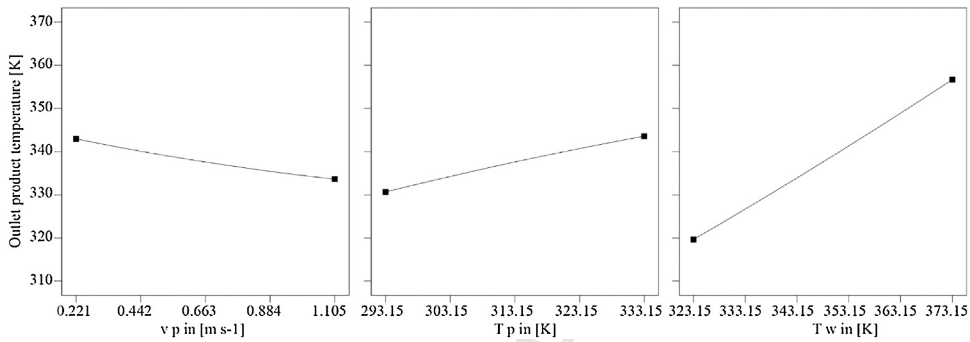

Fig. 15 – Tp,out one-factor response charts showing the sensitivity of the response and the effects of modifying one parameter at a time.

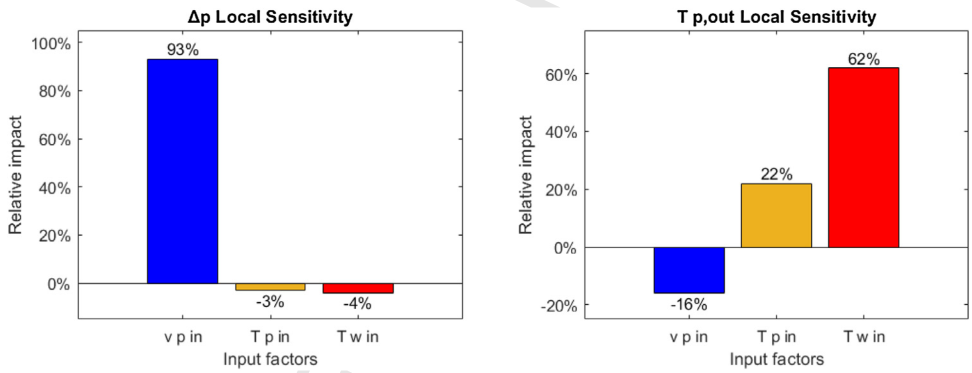

Fig. 16 – Relative impact of the input factors on the analyzed responses.

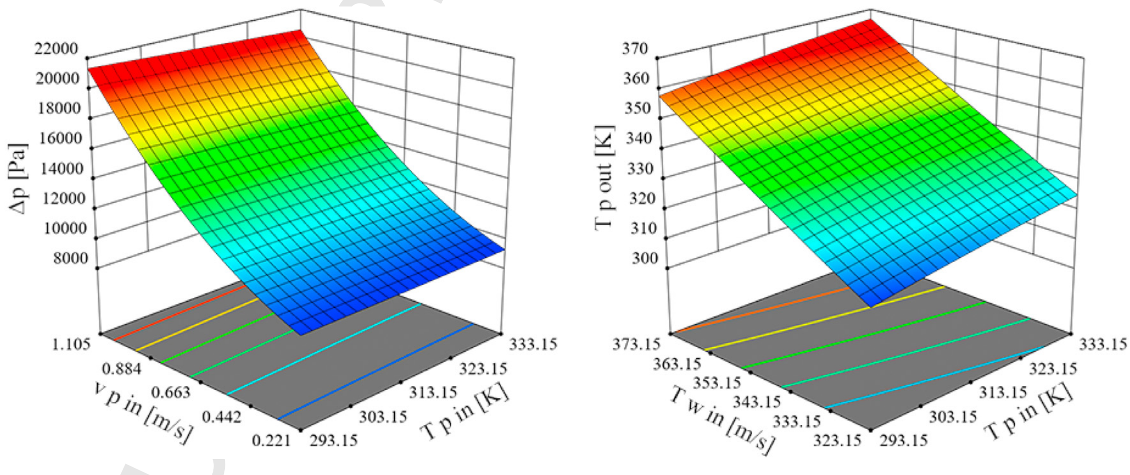

Fig. 17 – Response surfaces for pressure drop and outlet product temperature responses.

counter-current to water at a lower temperature, so it is subjected to cooling. It is important to notice that the response presents curvature, which is considered thanks to the choice of a second-order model.

The estimated responses for outlet product temperature are also represented as a function of $T_{p,in}$ and $T_{w,in}$, with $\upsilon_{p,in}$ values fixed at minimum, mean and maximum values (Fig. 20). As the flow rate increases, the product temperature increment

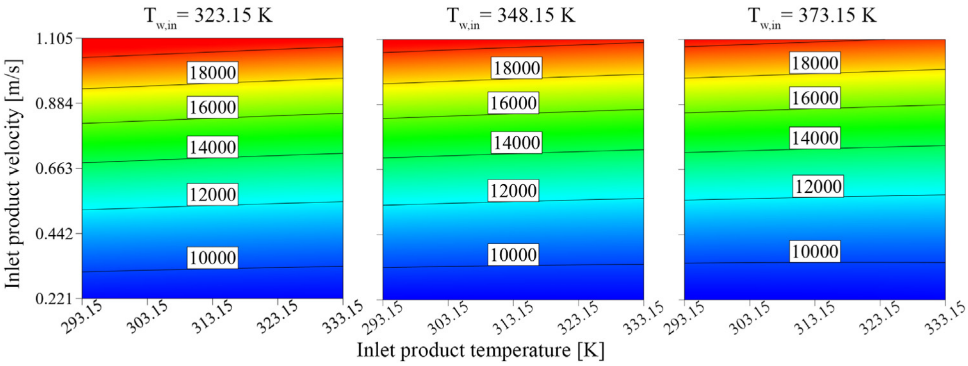

Fig. 18 – Response surface contour plots for pressure drop [Pa].

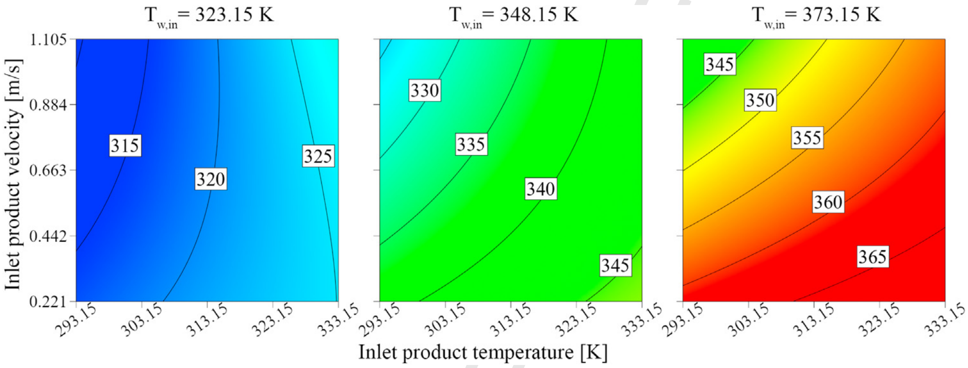

Fig. 19 – Response surface contour plots for outlet product temperature [K], as a combination of different levels of inlet product temperature and velocity.

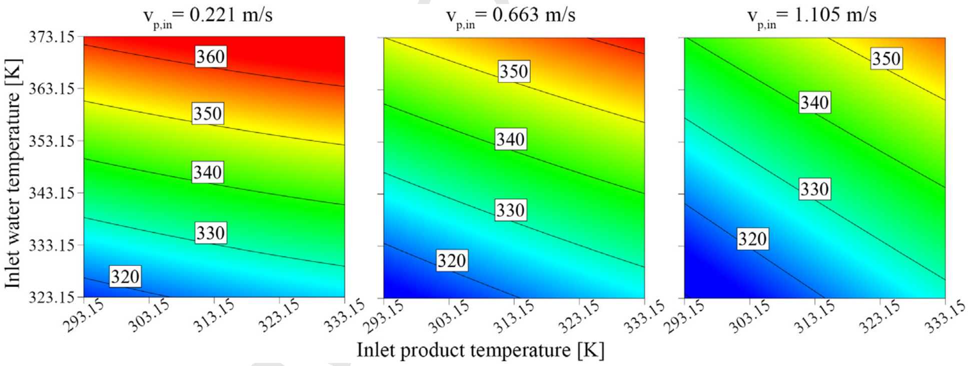

Fig. 20 – Response surface contour plots for outlet product temperature, as a combination of different levels of inlet product and water temperatures.

tends to decrease, and its dependence on the inlet product temperature becomes stronger.

3.3. *Experimental validation*

The results of the CFD simulations, and the generated Response Surface, were validated with an experimental campaign on the pilot plant. Measured and RS estimated outputs of interest are compared in Figs. 21 and 22. Plots of measured values of pressure and temperature are based on sensor readings that were acquired every 2 s with a Data Acquisition (DAQ) module and stored in a spreadsheet. RS estimated values were calculated with the final equations of the estimated response in terms of actual factors by multiplying the measured input factor readings by the coefficients of the quadratic model. The model was validated by comparing the measured outputs with the calculated ones. Thanks to the continuous acquisition of experimental data the comparison with the simulated results can be performed in every operating point where the

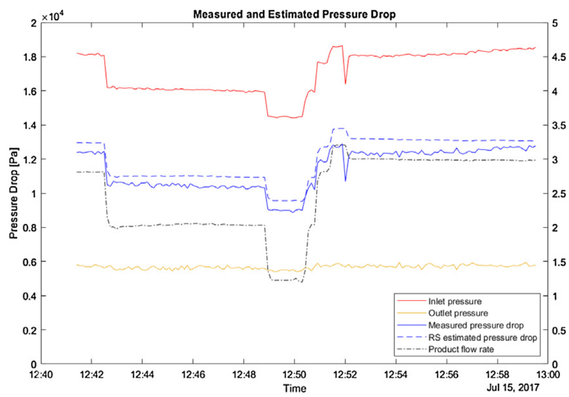

Fig. 21 – Experimental validation of the estimated pressure drop response.

input values lie within the considered range, rather than in a few selected validation points. As stated in Section 2.6, the fluid was continuously recirculated, so the only manually-

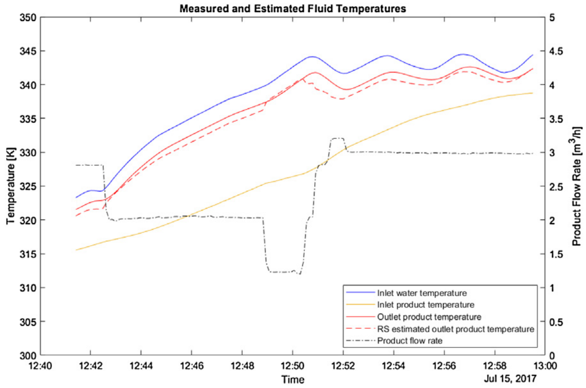

Fig. 22 – Experimental validation of the estimated outlet product temperature response.

set parameter was the product flow rate. A set-point value was established for the water temperature, which, therefore, tended to reach the desired value thanks to the automatic regulation of the opening percentage of the steam control valve. Due to the recirculating configuration the inlet product temperature rose continuously under the influence of the water temperature.

The experimental campaign was divided into three phases:

- 12:43–12:48 Constant flow rate (2 m^3/h), and constantly rising water and product temperatures. In accordance with the sensitivity analysis, the pressure drop appeared to be mainly influenced by flow rate and, therefore remained fairly constant throughout the entire phase.
- 12:48–12:52 Sudden significant changes in flow rate were induced to verify whether the reactivity of the real system was comparable to that of the model. Since the water temperature had not yet reached the defined set-point, the temperatures of both fluids were still increasing. The behavior of the real system was in agreement with the digital model, without significant delays or adaptation times.
- 12:52-13:00 Constant product flow rate (3 m^3/h) and water temperature oscillating around the set-point value. The temperature of the recirculated product approached the water temperature. Unlike the behavior observed in the first part of the test, a slight increase in pressure drop was observed in this phase. This can be explained by the onset of a time-dependent behavior of the Gellan gum solution. Time-dependent behavior of thickening agents under particular conditions has been investigated in the literature (Hernández et al., 2008; García et al., 2015). Further studies are necessary to investigate this aspect, which, however, is not strictly relevant to the objectives of this research.

The mean error, defined as the mean of punctual errors between the actual values and the estimated ones, was calculated to numerically evaluate the accuracy of the model. The Mean error was chosen for this purpose, since, as can be seen from Figs. 21 and 22, the difference between measured and estimated responses remains almost constant as the operating parameters vary.

$$e_{\Delta p} = \sum_{i=1}^{N} \frac{(p_{in,measured,i} - p_{out,measured,i}) - \Delta p_{RS,i}}{N} \quad (27)$$

Table 15 – Mean errors between measured and estimated outputs.

	$e_{\Delta p}$	$e_{\Delta T}$
e_{mean}	−628 Pa	0.85 K

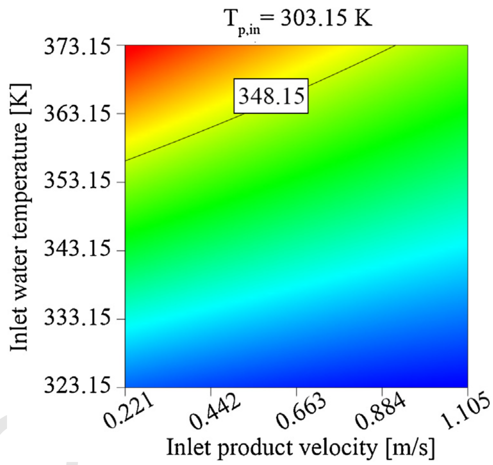

Fig. 23 – Outlet product temperature contour plot, with a highlighted iso-level at the desired pasteurization value.

$$e_{\Delta T} = \sum_{i=1}^{N} \frac{(T_{out,measured,i} - T_{in,measured,i}) - (T_{out,RS,i} - T_{in,measured,i})}{N} \quad (28)$$

where N is the number of sensor readings. The Mean errors for the two responses considered are as follows (Table 15).

The model, as can also be seen from Figs. 22 and 23, tends to overestimate the pressure drop by an average of 628 Pa, and to underestimate outlet product temperature by an average of 0.85 K.

In order to further improve the accuracy of this particular model, the calculated mean error values could be included in the final equations, as expected errors for the two responses. The final quadratic model equation for the estimation of outlet product temperature, therefore, would be:

$$\begin{aligned} T_{p,out} = &-86.24\,K + 5.26^* v_{p,in} + 1.05^* T_{p,in} + 0.47^* T_{w,in} \\ &+0.29^* v_{p,in}{}^* T_{p,in} - 0.32^* v_{p,in}{}^* T_{w,in} - (4.58e-04)\,^* T_{p,in}{}^* T_{w,in} \\ &+3.59^* v_{p,in}{}^2 - (1.22e-03)\,^* T_{p,in}{}^2 + (9.03e-04)\,^* T_{w,in}{}^2 \\ &+0.85\,K \end{aligned} \quad (29)$$

while the expected value of system pressure drop could be calculated from:

$$\begin{aligned} \Delta p = &\;21257.31\,Pa + 13422.97^* v_{p,in} - 40.41^* T_{p,in} - 42.84^* T_{w,in} \\ &-20.12^* v_{p,in}{}^* T_{p,in} - 15.05^* v_{p,in}{}^* T_{w,in} + 0.07^* T_{p,in}{}^* T_{w,in} \\ &+8208.07^* v_{p,in}{}^2 + 0.03^* T_{p,in}{}^2 + 0.03^* T_{w,in}{}^2 - 628\,Pa \end{aligned} \quad (30)$$

4. Discussion

Once the generated model is validated, RSM could be very useful in both predictive and operating phases as a support

Table 16 – RS defined Operating Points (OP) that allow obtaining the desired output product temperature.

	$v_{p,in}$ [m s^{-1}]	$T_{p,in}$ [K] Constraint	$T_{w,in}$ [K]	Δp [Pa]	$T_{p,out}$ [K] Target
OP 1	0.30	303.15	358.1	9740.72	348.15
OP 2	0.45	303.15	361.3	10897.11	348.15
OP 3	0.60	303.15	364.9	12491.70	348.15
OP 4	0.80	303.15	370.0	15159.22	348.15
OP 5	0.90	303.15	373.1	16867.94	348.15

Table 17 – Operating point that allows to reach the set-point temperature, while minimizing system pressure drop.

	$v_{p,in}$ [m s^{-1}]	$T_{p,in}$ [K] Constraint	$T_{w,in}$ [K]	Δp [Pa] Minimize	$T_{p,out}$ [K] Target
OP 6	0.22	303.15	356.3	9235.95	348.15

in the design and control of the plant respectively, allowing optimization of the process according to a series of goals and constraints.

In a predictive phase, in order to optimize the design of the plant and of the thermal process, it can be used to predict how the input parameter variations would affect the output variables. During the operating phase it allows identifying the possible operating points, defined as combinations of input processing parameters, that enable reaching a defined value for output of interest.

The case in which the *inlet product temperature* is known and a desired *outlet product temperature* has been defined is reported as an example. $T_{p,in}$ is set at 303.15 K, while the set-point $T_{p,out}$ is a pasteurization temperature of 348.15 K. A contour plot of the case is reported in Fig. 23, with $v_{p,in}$ and $T_{w,in}$ on the x and y axes, respectively. The colour range covers temperature values from a minimum of 315 K to a maximum of 363 K.

The chosen output temperature value is highlighted on the contour plot by an iso-level that identifies all the possible couples of inputs leading to the result requested.

Some of the possible operating points, calculated by means of a numeric optimization of the response surface, are reported in Table 16. In this optimization problem there is one goal ($T_{p,out}$=348.15 K) and one constraint ($T_{p,in}$=303.15 K).

If, in addition to the goal of reaching a target temperature, we aim to minimize the *system pressure drop*, the operating point that meets these requests can be calculated by means of a response optimization with two goals ($T_{p,out}$ = 348.15 K; $\Delta p_{opt} = \min(\Delta p)$) and one constraint ($T_{p,in}$ = 303.15 K).

The optimum operating point is defined as a combination of input parameters as follows (Table 17).

Any constraint on the input parameters that could be due to plant or product characteristics can be included in the optimization set-up so as to better adapt the solution to the real-life situation. Once they have been calculated, the product velocity and water temperature values obtained can be used to define the processing parameters of the pilot plant by setting the corresponding product flow rate and water temperature set-points on the control panel.

5. Conclusions

In this study, the behavior of a tubular heat exchanger has been reproduced by means of CFD simulations under different operating conditions thanks to a parametric study. Product flow rate, and inlet product and water temperatures were chosen as input parameters, while outlet product temperature and pressure drop across the heat exchanger were chosen as output parameters.

The product used in the study was characterized from a rheological point of view and its viscosity was modeled with a Power-law model, considering the temperature dependence through the Arrhenius equation. The rheological model appears to be more accurate at high temperatures ($T \geq 313.15$ K), because at low temperatures the pseudo-plastic behavior of the product changes and becomes more significant than at high temperatures.

A Response Surface was generated using a quadratic model, starting from the results of the parametric study. The results highlighted that the relative impact of $v_{p,in}$ on Δp was positive (93%), while higher $T_{p,in}$ and $T_{w,in}$ yielded lower pressure drop values across the heat exchanger (−3% and −4%, respectively). $T_{p,out}$ appeared to be positively influenced by inlet product (62%) and water (22%) temperatures, and negatively by $v_{p,in}$ (−16%). An ANOVA test showed that the quadratic model and the selected independent factors resulted to be significant for the estimation of both responses of interest.

The RS was validated through to a suitable experimental campaign. The Mean errors, defined as the mean of punctual errors between the actual values and the estimated ones, were calculated to numerically verify the model for the two responses of interest. Mean error values of 628 Pa and 0.85 K were obtained for pressure drop and outlet product temperature, respectively. These errors can be considered acceptable since, generally, in industrial applications, heat exchangers work with significant pressure drop and temperature variation so, in these conditions, the calculated mean error values become negligible. It is crucial, however, that the measured input data be accurate and reliable, otherwise incorrect information about the independent variables would lead to highly erroneous estimated results.

The results obtained can have significant implications in industrial applications as the method investigated allows generating a response surface that could be used as a Reduced-Order-Model of the plant, and which could be implemented to develop a Digital Twin (DT) of the heat exchanger when connected to its real-world counter-part by sensor measurements. The fact that the model was generated on the basis of steady-state simulations could reduce its accuracy in transient conditions which, however, are not the operating standard for this type of plant in common industrial applications characterized by stationary regime conditions. Further studies will have to be conducted to verify and investigate the applicability of the method to processes with more significant transients.

Please cite this article in press as: Lysova, N., et al., Optimization of an indirect heating process for food fluids through the combined use of CFD and Response Surface Methodology. Food Bioprod Process (2021), https://doi.org/10.1016/j.fbp.2021.10.010

The implementation of the DT would allow knowing how the system would behave at the measured conditions, evaluating any deviations and then making suitable adjustments to guarantee optimal performance. The model could also be used as a design tool, by setting a goal for the output values and calculating the possible combinations of inputs that lead to the desired result.

As stated in the Introduction, this modelling methodology could significantly improve the current state-of-the-art, since it would allow the results of the CFD simulations to be ready-to-use, thereby granting deeper knowledge and finer control of the system.

Declaration of interests

The authors declare that they have no known competing financial interests or personal relationships that could have appeared to influence the work reported in this paper.

References

Ansys, Inc, 2017a. (a). ANSYS Fluent Theory Guide, Release 18.0.
Ansys, Inc., 2017b. (c). DesignXplorer User's Guide, Release 18.0.
Arjmandi, H., Amiri, P., Saffari Pour, M., 2020. Geometric optimization of a double pipe heat exchanger with combined vortex generator and twisted tape: a CFD and response surface methodology (RSM) study. Therm. Sci. Eng. Prog. 18, 100514, http://dx.doi.org/10.1016/j.tsep.2020.100514.
Bottani, E., Vignali, G., Tancredi, G.P.C., 2020. A digital twin model of a pasteurization system for food beverages: tools and architecture. In: 2020 IEEE International Conference on Engineering, Technology and Innovation (ICE/ITMC), pp. 1–8, http://dx.doi.org/10.1109/ice/itmc49519.2020.9198625.
Box, G.E.P., Wilson, K.B., 1951. On the experimental attainment of optimum conditions. J. R. Stat. Soc. Ser. B 13 (1), 1–38, http://dx.doi.org/10.1111/j.2517-6161.1951.tb00067.x.
Chhabra, R.P., Richardson, J.F., 1999. ch.6 Heat Transfer Characteristics of Non-Newtonian Fluids in Pipes. Non-Newtonian Flow in the Process Industries. Butterworth-Heinemann, pp. 260–288, http://dx.doi.org/10.1016/b978-075063770-1/50007-5.
Córcoles, J.I., Marín-Alarcón, E., Almendros-Ibáñez, J.A., 2020. (b). Heat transfer performance of fruit juice in a heat exchanger tube using numerical simulations. Appl. Sci. 10 (2), 648, http://dx.doi.org/10.3390/app10020648.
D'Addio, L., Di Natale, F., Budelli, A., Nigro, R., 2014. CFD simulation for the pasteurization of fruit puree with pieces. Chem. Eng. Trans. 39, 1699–1704, http://dx.doi.org/10.3303/CET1439284.
Dantas, J.A.T.A., Gut, J.A.W., 2018. Modeling sterilization value and nutrient degradation in the thermal processing of liquid foods under diffusive laminar flow with associations of tubular heat exchangers. J. Food Process Eng. 41 (8), e12897, http://dx.doi.org/10.1111/jfpe.12897.
Fialho, A.M., Moreira, L.M., Granja, A.T., Popescu, A.O., Hoffmann, K., Sá-Correia, I., 2008. Occurrence, production, and applications of Gellan: current state and perspectives. Appl. Microbiol. Biotechnol. 79 (6), http://dx.doi.org/10.1007/s00253-008-1496-0.
García, M.C., Alfaro, M.C., Muñoz, J., 2015. Yield stress and onset of nonlinear time-dependent rheological behaviour of gellan fluid gels. J. Food Eng. 159, 42–47, http://dx.doi.org/10.1016/j.jfoodeng.2015.02.024.
Han, H.-Z., Li, B.-X., Wu, H., Shao, W., 2015. Multi-objective shape optimization of double pipe heat exchanger with inner corrugated tube using RSM method. Int. J. Therm. Sci. 90, 173–186, http://dx.doi.org/10.1016/j.ijthermalsci.2014.12.010.
Hernández, M.J., Dolz, J., Delegido, J., Cabeza, C., Dolz, M., 2008. Thixotropic behavior of salad dressings stabilized with modified starch, pectin, and gellan gum. Influence of temperature. J. Dispers. Sci. Technol. 29 (2), 213–219, http://dx.doi.org/10.1080/01932690701707191.
Jha, S.N., Prasad, S., 1996. Determination of processing conditions for gorgon nut (Euryale ferox). J. Agric. Eng. Res. 63 (2), 103–111, http://dx.doi.org/10.1006/jaer.1996.0012.
Jouki, M., Mortazavi, S.A., Yazdi, F.T., Koocheki, A., 2014. Optimization of extraction, antioxidant activity and functional properties of quince seed mucilage by RSM. Int. J. Biol. Macromol. 66, 113–124, http://dx.doi.org/10.1016/j.ijbiomac.2014.02.026.
Khodashenas, M., Jouki, M., 2020. Optimization of stabilized probiotic Doogh formulation by edible gums and response surface methodology: assessment of stability, viability and organoleptic attributes. J. Food Sci. Technol. 57 (9), 3201–3210, http://dx.doi.org/10.1007/s13197-020-04351-3.
Kola, P.V.K.V., Pisipaty, S.K., Mendu, S.S., Ghosh, R., 2021. Optimization of performance parameters of a double pipe heat exchanger with cut twisted tapes using CFD and RSM. Chem. Eng. Process. Process. Intensif. 163, 108362, http://dx.doi.org/10.1016/j.cep.2021.108362.
LaNasa, P.J., Upp, E.L., 2014. ch.2 Basic Flow Measurement Laws. Fluid Flow Measurement., pp. 19–29, http://dx.doi.org/10.1016/b978-0-12-409524-3.00002-2.
Liu, S., Huang, W., Bao, Z., Zeng, T., Qiao, M., Meng, J., 2021. Analysis, prediction and multi-objective optimization of helically coiled tube-in-tube heat exchanger with double cooling source using RSM. Int. J. Therm. Sci. 159, 106568, http://dx.doi.org/10.1016/j.ijthermalsci.2020.106568.
Maloney, N., Harrison, M., 2016. ch.8 Advanced Heating Technologies for Food Processing. Innovation and Future Trends in Food Manufacturing and Supply Chain Technologies., pp. 203–256, http://dx.doi.org/10.1016/b978-1-78242-447-5.00008-3.
Maradiya, C., Vadher, J., Agarwal, R., 2018. The heat transfer enhancement techniques and their thermal performance factor. Beni-Suef Univ. J. Basic Appl. Sci. 7 (1), 1–21, http://dx.doi.org/10.1016/j.bjbas.2017.10.001.
Menter, F.R., 1994. Two-equation eddy-viscosity turbulence models for engineering applications. AIAA J. 32 (8), 1598–1605, http://dx.doi.org/10.2514/3.12149.
Metzner, A.B., Reed, J.C., 1955. Flow of non-Newtonian fluids—correlation of the laminar, transition, and turbulent-flow regions. AIChE J. 1 (4), 434–440, http://dx.doi.org/10.1002/aic.690010409.
Mishra, P., Ein-Mozaffari, F., 2021. Intensification of suspension of solid particles in non-Newtonian fluids with coaxial mixers. Chem. Eng. Process. Process. Intensif. 168, art. no. 108553.
Montgomery, D.C., 2001. ch.11, Response Surface Methods and Other Approaches to Process Optimization. Design and Analysis of Experiments, 5th edition. John Wiley and Sons, pp. 427–510.
Perone, C., Romaniello, R., Leone, A., Catalano, P., Tamborrino, A., 2021. CFD analysis of a tubular heat exchanger for the conditioning of olive paste. Appl. Sci. 11 (4), 1858, http://dx.doi.org/10.3390/app11041858.
Rinaldi, M., Cordioli, M., Alinovi, M., Malavasi, M., Barbanti, D., Mucchetti, G., 2018. Development and validation of CFD models of thermal treatment on milk whey proteins dispersion in batch and continuous process condition. Int. J. Food Eng. 14 (9–10), http://dx.doi.org/10.1515/ijfe-2018-0142.
Shenoy, A., 2018. ch.8 Turbulent Forced and Mixed Convection in Internal Flows of Non-Newtonian Fluids. Heat Transfer to Non-Newtonian Fluids. Wiley-VCH, pp. 131–162, http://dx.doi.org/10.1002/9783527811687.
Singh, R.P., Heldman, D.R., 2014. ch.4 Heat Transfer in Food Processing. Introduction to Food Engineering. Academic Press, pp. 265–419, http://dx.doi.org/10.1016/b978-0-12-398530-9.00004-8.
Steffe, J.F., 1996. ch.1, Introduction to Rheology. Rheological Methods in Food Process Engineering. Freeman Press, pp. 1–91.
Tagliavini, G., Defraeye, T., Carmeliet, J., 2019. Multiphysics modeling of convective cooling of non-spherical,

Please cite this article in press as: Lysova, N., et al., Optimization of an indirect heating process for food fluids through the combined use of CFD and Response Surface Methodology. Food Bioprod Process (2021), https://doi.org/10.1016/j.fbp.2021.10.010

multi-material fruit to unveil its quality evolution throughout the cold chain. Food Bioprod. Process. 117, 310–320.

Verboven, P., Defraeye, T., Datta, A.K., Nicolai, B., 2020. Digital twins of food process operations: the next step for food process models? Curr. Opin. Food Sci. 35, 79–87.

Yolmeh, M., Jafari, S.M., 2017. Applications of response surface methodology in the food industry processes. Food Bioproc. Technol. 10 (3), 413–433, http://dx.doi.org/10.1007/s11947-016-1855-2.

Yu, C., Chen, J., Zeng, M., Gao, B., 2019. Numerical study on turbulent heat transfer performance of a new parallel flow shell and tube heat exchanger with sinusoidal wavy tapes using RSM analysis. Appl. Therm. Eng. 150, 875–887, http://dx.doi.org/10.1016/j.applthermaleng.2019.01.043.

Please cite this article in press as: Lysova, N., et al., Optimization of an indirect heating process for food fluids through the combined use of CFD and Response Surface Methodology. Food Bioprod Process (2021), https://doi.org/10.1016/j.fbp.2021.10.010